Supporting Information

Overcoming artificial broadening in Gd^{3+}-Gd^{3+} distance distributions arising from dipolar pseudo-secular terms in DEER experiments

Marie Ramirez Cohen, Veronica Frydman, Petr Milko, Mark A. Iron, Elwy H. Abdelkader, Michael D. Lee, James D. Swarbrick, Arnold Raitsimring, Gottfried Otting, Bim Graham, Akiva Feintuch, Daniella Goldfarb

Contents

S1. Primary DEER data model compound 7.

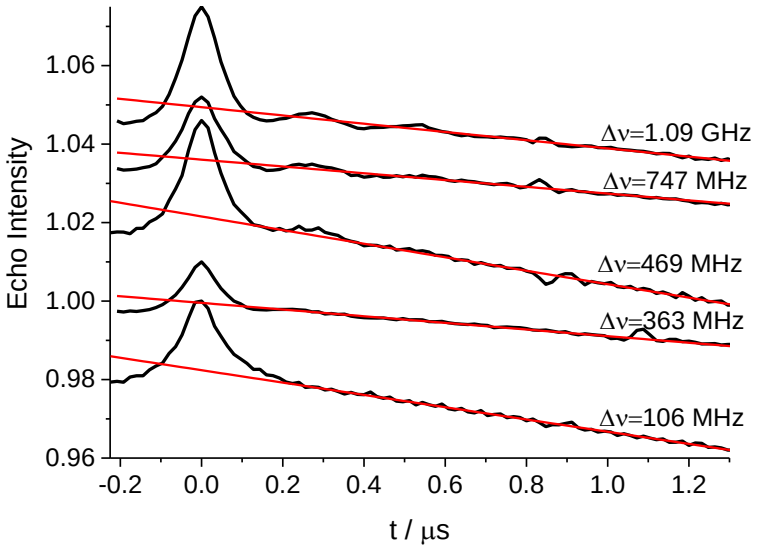

Fig. S1 Primary DEER traces of the *bis*-Gd^{3+}-DOTA model compound **7.** The red lines show the background decay for the traces. The data were normalized to 1 and the traces are shifted with respect to each other for clarity.

S2. Ka-band DEER data

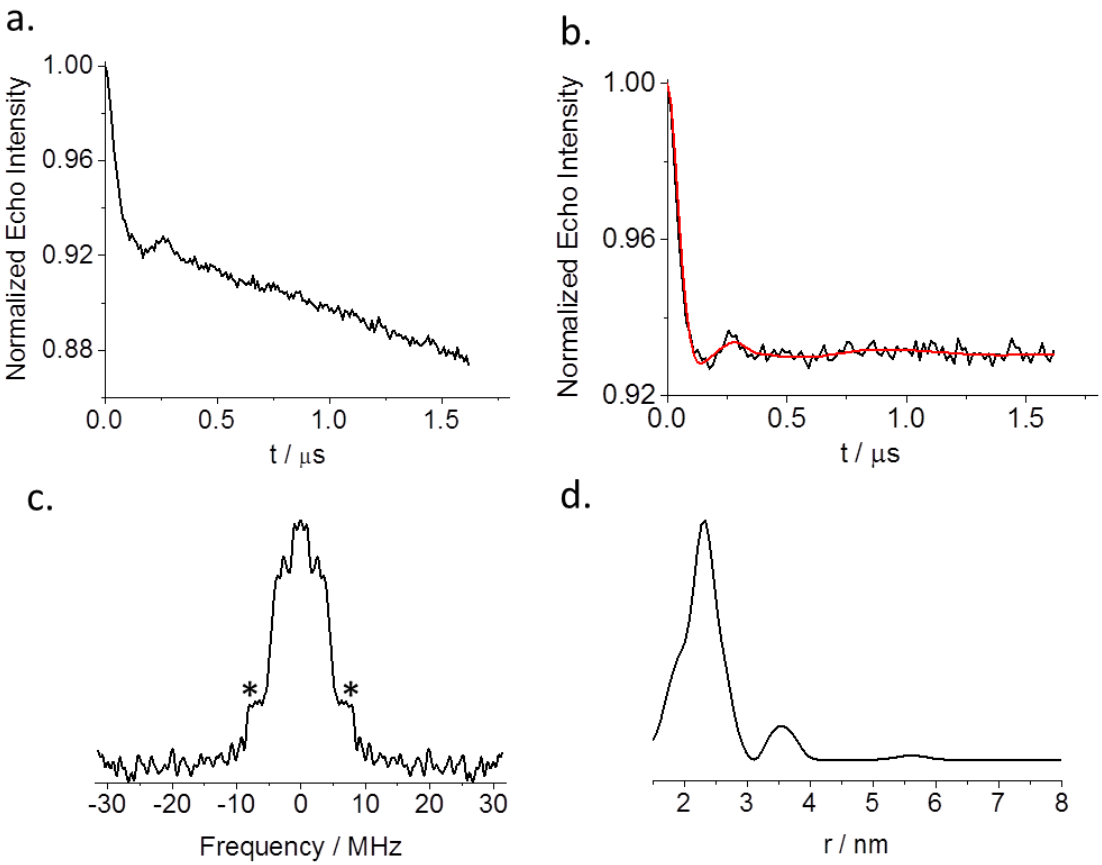

Fig. S2 Ka-band DEER data of the *bis*-Gd^{3+}-DOTA model compound **7** measured on a home-built Ka-band spectrometer[1] using a dielectric resonator with a resonance frequency of 34.448 GHz and additional secondary resonances between 35-36 GHz.[2] **(a)** Primary DEER trace. The measurement parameters were: T = 15 K; $\Delta\nu$ = 728 MHz; pulse durations of the observe pulses: $t_{\pi/2}$ = 6 ns, t_{π} = 12 ns; duration of the pump pulse: t_{π} = 10 ns; τ = 250 ns; τ_1 = 2.6 µs; repetition time = 1 ms. **(b)** DEER trace after background removal. **(c)** Fourier transform of (**b**). The parallel singularities, marked with stars, also have contributions from ^{2}H nuclear modulations. **(d)** Distance distribution calculated by DeerAnalysis.

S3. DFT Geometry Optimizations

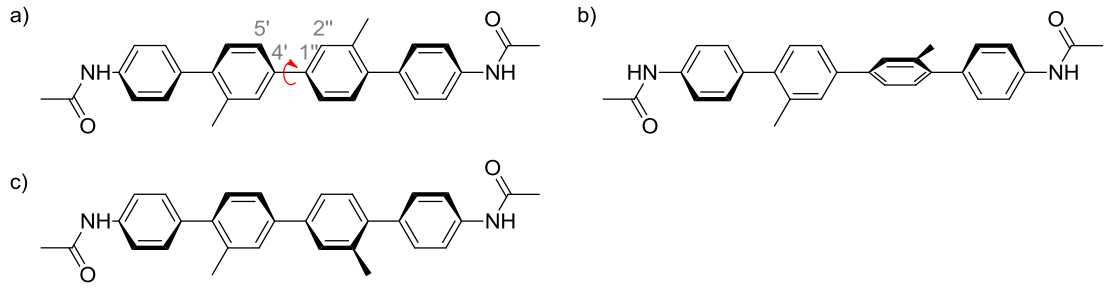

Scheme S1. Different conformations of the N,N'-(2',3''-dimethyl-[1,1':4',1'':4'',1'''-quaterphenyl]-4,4'''-diyl)diacetamide linker. The panels **a)** to **c)** display conformations with the methyl groups in the *trans*, perpendicular and *cis* positions, respectively.

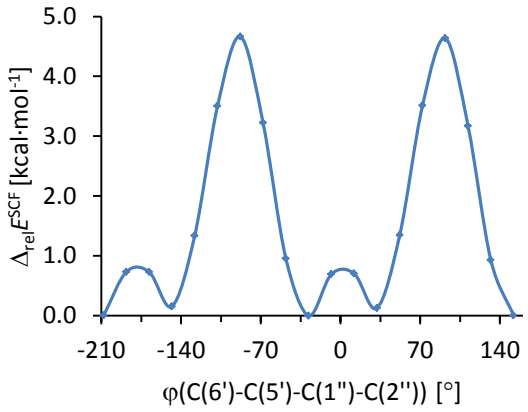

Fig. S3 Energy profile of the rotation by the dihedral angle φ defined by the atoms C(5')-C(4')-C(1'')-C(2''). The first minimum located at φ = -208° corresponds to a configuration with the two methyl substituents in the *trans* position (Scheme S1) and the planes of the two ring moieties rotated by 28°. The energy rises as the dihedral angle increases and reaches a local maximum at φ = -188°. The increase in energy is caused by increased repulsive interaction between the hydrogens attached to C(5') and C(2'') as shown by non-covalent interaction (NCI) plots (Fig. S4). This repulsive interaction acts against coplanarity of the two aromatic rings. In the second energy minimum, both methyl substituents are *cis* (Scheme 1c; φ = -28°) and a local maximum is observed for φ = 12°. The two large maxima correspond to structures where the aromatic rings are perpendicular to each other.

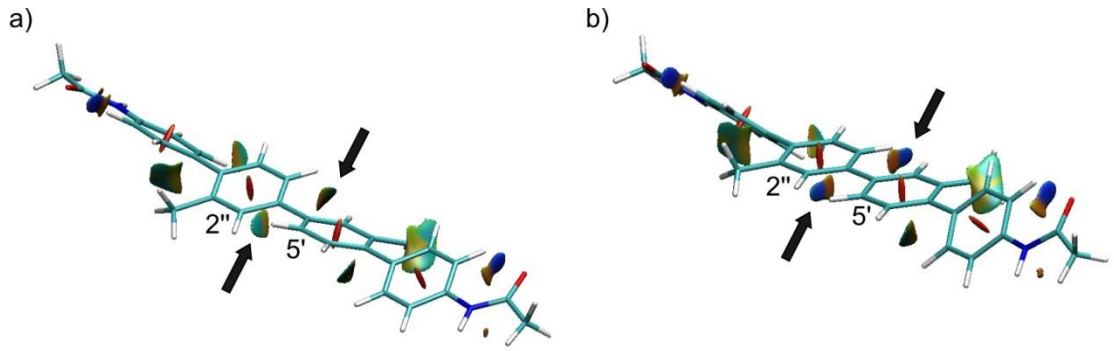

Fig. S4 NCI plots of the N,N'-(2',3"-dimethyl-[1,1':4',1":4",1"'-quaterphenyl]-4,4"'-diyl)diacetamide linker. **a)** NCI plot for φ(C(5')-C(4')-C(1")-C(2")) = -211°. The non-covalent interactions are color-coded as follows: weak repulsion: green; strong repulsion: red; strong attraction: blue. The black arrows point to isosurfaces that identify repulsive interactions between C(5') and C(2") of the middle rings. **b)** Same as **a)**, except for φ(C(5')-C(4')-C(1")-C(2")) = -180°.

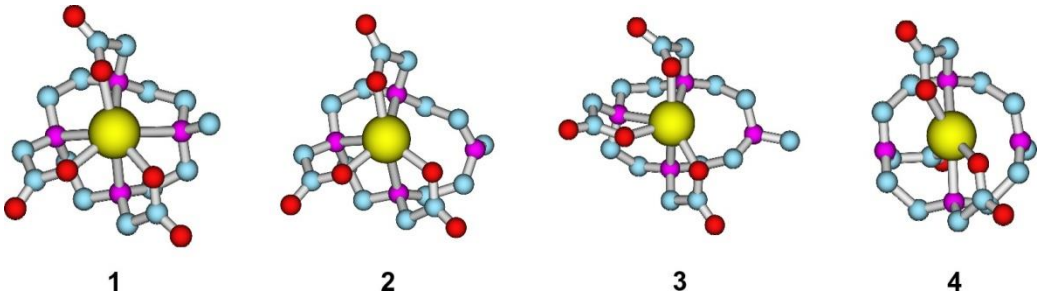

Figure S5. Optimized structure of 2,2',2"-(10-methyl-1,4,7,10-tetraazacyclododecane-1,4,7-triyl)triacetate lanthanum(III). Color scheme: C: blue, N: purple, O: red, La: yellow. The hydrogen atoms are omitted for clarity. In principle, it is possible to start from the coordinated amide complex. However, by building up in stages (and it should be expected that the energy profiles of the linker should not change much upon adding the La(DO3A) groups, we reduce the complexity of the final problem and reduce the computational time required.

Table S1. Relative energies of isomers of 2,2',2''-(10-methyl-1,4,7,10-tetraazacyclododecane-1,4,7-triyl)triacetate lanthanum(III).

isomer	$\Delta_{rel}E^{SCF}$, [kcal·mol^{-1}]
1	0.0
2	21.0
3	25.7
4	76.9

S4. EPR simulations and primary DEER data for T4 lysozyme

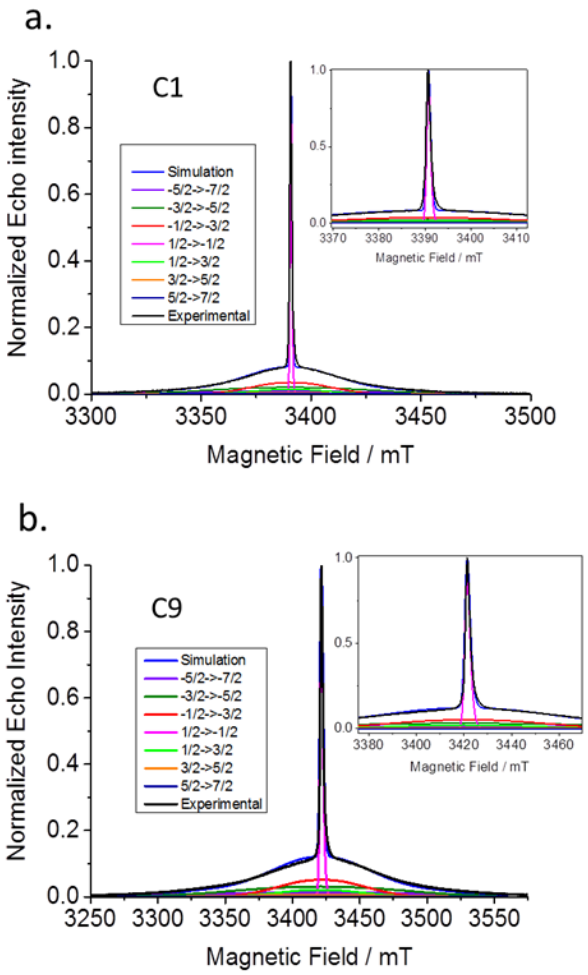

Fig. S6 W-band ED-EPR spectra recorded at 10 K of T4 lysozyme A93C/N140C ligated with **a)** C1-Gd^{3+} and **b)** C9-Gd^{3+} tags. The EPR spectra were simulated with the contributions of the individual transitions according to the colors in the legends. The simulations assumed a bimodal distribution with the Gaussian centers at D and $-D$ and a width of $|D/2|$. E/D was varied from 0 to 1/3 with a probability of $p(E/D) \propto E/D\text{-}2(E/D)^2$. The values for the C1-$Gd^{3+}$ and C9-Gd^{3+} tags were 450 MHz and 800 MHz, respectively. The inserts show enlargements of the central transitions.

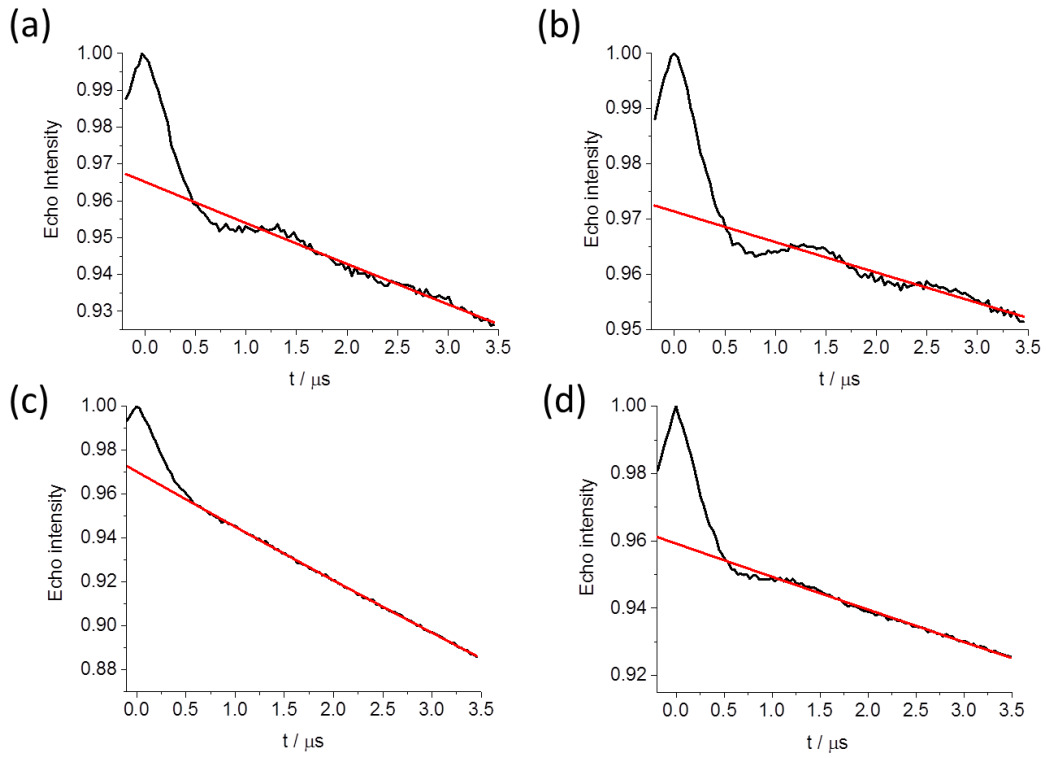

Fig. S7 W-band primary DEER traces (10 K) of T4 lysozyme A93C/N140C ligated with **(a), (c)** C1-Gd^{3+} and **(b), (d)** C9-Gd^{3+} tags. **(a)** and **(b)** were recorded with the dual mode cavity and the pump and detect frequencies separated by $\Delta\nu$=898 MHz and 636 Mhz, respectively, while **(c)** and **(d)** were recorded with the single mode cavity and a separation of $\Delta\nu$=100 MHz. The red line shows the background decay for both traces.

1 A. V. Astashkin, J. H. Enemark and A. Raitsimring, *Concepts Magn. Reson. Part B Magn. Reson. Eng.*, 2006, **29 B**, 125–136.

2 A. Raitsimring, A. Astashkin, J. H. Enemark, A. Blank, Y. Twig, Y. Song and T. J. Meade, *Appl. Magn. Reson.*, 2012, **42**, 441–452.